Title:

Strand-swapping in the LolA-like protein GerS promotes the allosteric activation of a bacterial amidase in *Clostridioides difficile*

Authors:

Jacob M. Bouchier[1] and Aimee Shen[1]

Affiliations:

[1]Department of Molecular biology and Microbiology, Tufts University School of Medicine, Boston, MA, USA

Running head: Strand-swapping in GerS promotes the allosteric activation of CwlD

[#]Corresponding author:

aimee.shen@tufts.edu

(617)636-3792

Abstract:

GerS is a key lipoprotein regulator of *Clostridioides difficile* spore germination that shares structural, but not sequence, similarity to LolA in Gram-negative bacteria. GerS and LolA have vastly different biological roles: LolA functions in the trafficking of lipoproteins across the periplasmic space to the outer membrane of Gram-negative bacteria, while GerS allosterically activates the germination-specific amidase CwlD in endospore-forming Gram-positive bacteria. Here, we explore the diversity of LolA-like proteins across bacteria and reveal that GerS homodimer formation is a conserved feature of Peptostreptococcaceae family orthologs. Since dimerization of *C. difficile* GerS occurs via strand-swapping, we sought to investigate the functional importance of its strand swap by identifying mutations that alter the GerS dimer:monomer equilibrium. Our analyses reveal that $GerS^{K71R}$ and $GerS^{N74L}$ substitutions in the strand-swap hinge of GerS stabilize the homodimer, while a $GerS^{T72P}$ substitution promotes monomer formation. Conversely, substituting the highly conserved proline at the equivalent site in LolA for threonine converts LolA from a monomer to a homodimer. Since our data indicate that destabilizing the GerS dimer impairs both GerS:CwlD binding *in vitro* and CwlD function in *C. difficile*, strand-swapped dimer formation in LolA-like proteins enhances their affinity for their binding partners. These data are consistent with analyses of equivalent LolA mutants in *E. coli* and thus provide new insight into the evolution and specialization of this intriguing group of proteins across the bacterial domain.

Introduction

The InterPro homologous superfamily "Prokaryotic lipoproteins and lipoprotein localization factors" (PLLLF) encompasses a group of structurally similar, widely distributed across the bacterial domain. While some proteins of this group function as anti-sigma factors [1,2], most have been implicated as chaperones involved in transport across the periplasmic space of diderm bacteria. LolA, the archetypal PLLLF protein, functions within the Lol system (LolABCDE) to facilitate lipoprotein trafficking across the periplasm in diderm bacteria [3–9]. Similarly, LppX [10], LprG [11], and LprF [12] transport various glycolipids to the *Mycobacterium* cell wall.

In contrast, PLLLF proteins in endospore-forming monoderm bacteria seem to have evolved specialized roles in sporulation and germination. For example, SsdC from *Bacillus subtilis* forms a ring-like structure in the forespore that functions in the development of spore shape [13] and GerS regulates spore germination in *Clostridioides difficile* [14]. Spore germination depends on the degradation of the cortex, a protective layer of modified peptidoglycan, by cortex lytic enzymes [15,16]. Cortex lytic enzymes specifically bind to the spore-specific peptidoglycan modification, muramyl-δ-lactam (MAL) [20], which limits their degradative activities to the cortex layer. The generation of MAL involves the coordinated activities of the germination-specific amidase CwlD and the peptidoglycan deacetylase PdaA [21–24].

While *B. subtilis* CwlD has intrinsic activity, *C. difficile*, CwlD requires an additional factor to license its activity, the GerS lipoprotein [25,26]. GerS forms a 1:1 complex with CwlD and allosterically activates CwlD's amidase activity by stabilizing the binding of its Zn^{2+} cofactor [26]. This interaction is essential for germination, as deletion of *gerS* abolishes spore germination in *C. difficile* [14] and disrupting a salt bridge formed between aspartate 106 of GerS and arginine

169 of CwlD reduces germination [26]. However, despite the GerS D106R substitution significantly reducing binding to CwlD *in vitro*, the reduction in germination is relatively subtle, [26], suggesting that additional factors beyond the salt bridge regulates the GerS:CwlD interaction.

The crystal structure of the GerS:CwlD complex revealed that GerS dimerizes via a strand-swap mechanism [26]. Strand swapping, a specific form of domain swapping, is a dimerization mechanism in which β-strands are exchanged between two proteins [27]. First characterized in diphtheria toxin [28,29], domain swapping has since been described in many proteins [30–36] across all domains of life. To our knowledge, *C. difficile* GerS is the only known PLLLF protein that naturally dimerizes via a strand swap mechanism. In contrast, LolA from *Escherichia coli* can be induced to strand swap via a mutation (F68E, published as F47E) [37,38], but this mutation is toxic to growth because $LolA^{F68E}$ binds LolC too tightly and prevents proper lipoprotein trafficking to the outer membrane [38]. Based on these observations and the finding that strand-swapping promotes adhesive interactions for cadherins, we hypothesized that GerS strand swapping functions to increase its affinity for CwlD. In this study, we test the role of the strand swap in GerS homodimerization, interaction with CwlD, and regulation of spore germination. By identifying specific mutations that shift the GerS dimer:monomer equilibrium, we provide molecular insight into the mechanisms governing strand swapping and the functional importance of these structures in regulating adhesive interactions.

Results

PLLLF proteins maintain low sequence identity but high sequence similarity and structural similarity.

With the goal of identifying the underlying and shared features between GerS and the rest of the PLLLF group, we initially explored the evolutionary relatedness of proteins within the group. We found that heuristic search methods, such as BLASTp, were inadequate for identifying members of this group. Instead, we employed probabilistic searches using InterPro and structural searches using FoldSeek to identify which major bacterial classes contain bacteria that encode PLLLF proteins [39–42]. We then generated a phylogenetic tree using core genes across species and labeled which major bacterial classes have species that encode PLLLF proteins (Supplemental Figure 1). Remarkably, we found that PLLLF proteins are widespread across the bacterial domain, suggesting a shared ancestry. Further, we found that the presence of PLLLF proteins is independent of whether the bacteria are monoderms or diderms, suggesting that not all PLLLF proteins function in a similar way to LolA.

Using AlphaFold 3, we predicted the structure of 17 representative PLLLF proteins and aligned them using DALI [43,44]. A dendrogram generated by the number of differences between each structure shows structural similarity of representatives within phyla with the exception of the three representatives of the phylum Pseudomanodota (formerly Proteobacteria) (Figure 1A). We also visualized the structural alignment in UCSF ChimeraX and observed that the structures are strikingly similar to one another (Figure 1B) [45]. Using the DALI structural alignment, we also compared sequence identity and sequence similarity. These analyses revealed that despite the sequence identity being low across the PLLLF group, their sequence similarity is high (Figure 1C). Together, these observations indicate that PLLLF proteins are highly conserved and suggest that they share evolutionary ancestry, although they likely evolved specialized roles within diderms vs. monoderms.

GerS strand-swapping is unique among characterized PLLLF proteins.

While AlphaFold3 predicts that GerS adopts a structure remarkably similar to other PLLLF proteins, the GerS-CwlD crystal structure shows that GerS forms a homodimer via a strand-swap mechanism [26]. Crystal structures of other PLLLF proteins, ranging across several bacterial classes, suggest that PLLLF proteins exist either as monomers or heterodimers with other proteins but rarely as homodimers [3,5,10,11,46,47].

While LolA does not form homodimers naturally, a single substitution of phenylalanine to glutamate at residue 68 (F68E, previously published as F47E based on numbering from the lipobox) is sufficient to induce homodimerization (Supplemental Figure 2). The $LolA^{F68E}$ variant binds its interacting partner LolC with higher affinity, which reduces its affinity for the lipoproteins substrates that LolA normally shepherds across the periplasm. As a result, the $LolA^{F68E}$ is toxic to *E. coli* [37,38]. Notably, GerS is a sporulation-induced protein that is not essential during vegetative growth, although its binding to CwlD is critical for spore germination. Thus, we hypothesized that GerS dimerization evolved in monoderm sporulating bacteria, which do not require a LolA-like lipoprotein chaperone because they lack an outer membrane, to stabilize binding to CwlD and promote CwlD binding to its Zn^{2+} co-factor.

Dimerization is conserved in GerS orthologs of the Peptostreptococcaceae family.

To explore this possibility, we first assessed the conservation of *gerS* among the Firmicutes, the only known class to contain endospore-forming bacteria like *C. difficile* and *Bacillus subtilis*. To avoid issues associated with identifying PLLLF proteins through heuristic methods like BLASTp, we instead used synteny-based searches such as GeCoViz and BioCyc genome alignment to find GerS orthologs within the Firmicutes and confirmed each through structural alignment of AlphaFold3-predicted structures in ChimeraX (Figure 2A; Supplemental Figure 3A) [44,45,48,49].

142 Six orthologs were selected from Firmicutes that sporulate and encode a GerS ortholog for
143 further characterization. To investigate dimerization, each ortholog was expressed in *E. coli* and
144 purified for analysis via size-exclusion chromatography (SEC). The SEC trace of GerS from
145 *Clostridioides difficile* revealed two distinct peaks, which represent the monomeric and
146 homodimeric forms of the protein ([26], Figure 2B; Supplemental Figure 4). Notably, two other
147 Firmicutes, *Paraclostridium bifermentans* and *Paraclostridium sordellii*, exhibited similar SEC
148 profiles, indicating that they also form homodimers. In contrast, GerS orthologs from *Clostridium*
149 *aceticum*, *Gottschalkia acidurici*, and *Clostridium perfringens* displayed a single peak
150 corresponding to the monomeric form. Since *P. bifermentans* and *P. sordellii* are members of
151 the Peptostreptococcaceae family like *C. difficile*, unlike the other species tested, these data
152 strongly suggest that GerS dimerization is specific to the Peptostreptococcaceae family.
153
154 We also identified GerS orthologs in the Bacilli class, but they are distinguished by an additional
155 domain of unknown function (DUF4367). We purified the *Bacillus subtilis* ortholog, previously
156 published as SsdC [13], with and without the DUF4367 domain and analyzed the two variants
157 via SEC. Although both traces had two peaks, Coomassie staining of earlier eluting fraction
158 showed additional bands beyond the expected size for SsdC (Supplemental Figure 4B-C),
159 indicating that SsdC primarily exists as a monomer *in vitro* and that the DUF4367 domain does
160 not play a role in SsdC dimerization. Thus, GerS dimerization is limited to the
161 Peptostreptococcaceae family.
162
163 **Mutations in the strand-swap hinge alter GerS dimer stability.**
164 To determine the role of the strand swap in regulating GerS dimerization and function, we aimed
165 to identify mutations that destabilize the GerS dimer. Previous studies have shown that
166 mutations that disrupt the 'hinge' region of the swapped strand can prevent dimerization (Figure
167 3A) [34,35,50–52]. While these studies have also shown that it can be difficult to predict which

168 residue will alter a given dimer:monomer equilibrium, we reasoned that replacing the hinge of
169 GerS with the equivalent sequence found in a monomeric PLLLF protein like LolA might prevent
170 GerS dimerization. To this end, we used AlphaFold3 to predict the monomeric structure of GerS
171 and aligned it with the LolA crystal structure (PDB 1IWL). This alignment revealed that the GerS
172 strand-swap hinge, Lys71-Thr72-Asp73-Asn74 (KTDN), lies in a similar position to LolA Arg71-
173 Pro72-Asn73-Leu74 (RPNL; Figure 3B). We then tested the effect of replacing individual amino
174 acids in the *C. difficile* GerS hinge with the analogous residues in the *E. coli* LolA region.
175 Intriguingly, replacing Thr72 with Pro increased the proportion of GerS in the monomeric form,
176 while replacing the Lys71 with Arg and Asn74 with Leu increased the dimeric form (Figure 3C;
177 Supplemental Figure 5A). In contrast, $GerS^{D73N}$ precipitated quickly after purification and co-
178 purified with a likely chaperone protein from *E. coli* [53] (Supplemental Figure 5B), strongly
179 suggesting that the substitution destabilized GerS.
180
181 Since the $GerS^{K71R}$ and $GerS^{N74L}$ variants favored the dimeric form relative to WT GerS (Figure
182 3C-D), we purified the dimeric fractions and re-analyzed them by SEC to compare the relative
183 stabilities of the GerS homodimers formed by each variant. The re-purified $GerS^{K71R}$ or $GerS^{N74L}$
184 variants again showed a higher dimer-to-monomer ratio than WT GerS (Supplemental Figure
185 6A-B), indicating that the K71R and N74L substitutions enhance the stability of the GerS
186 homodimer structure.
187
188 **Proline substitutions in the strand-swap hinge destabilize the GerS homodimer.**
189 Since $GerS^{T72P}$ favored the monomeric form compared to WT GerS (Figure 3C-D), we next
190 tested the effect of changing the other hinge residues to proline. Previous studies have found
191 that introducing prolines into the strand-swap hinge affects dimerization in a wide range of
192 proteins across all domains of life [34,35]. For example, highly conserved prolines in the loops
193 of *Mycobacterium tuberculosis* BlaC maintain BlaC in a monomeric and functional form,

194 whereas substitutions of these residues result in dimerization and loss of function [54]. When
195 the other hinge residues of GerS were replaced with proline (K71P, D73P, and N74P), all three
196 substitutions appeared to destabilize GerS because they copurified with several *E. coli* proteins
197 that are likely chaperones (Figure 4B; Supplemental Figure 7B). Thus, the location of the proline
198 substitution is critical for regulating the GerS dimer-to-monomer equilibrium.
199
200 Consistent with this finding, analysis of the conservation of hinge prolines among PLLLF
201 proteins using the DALI alignment revealed that three proline residues are highly conserved
202 among this family, and each of these prolines correspond to structural loops in PLLLF proteins
203 (Supplemental Figure 7A). Notably, GerS contains two of these conserved prolines but not the
204 conserved proline at residue 72. Together these observations highlight how a proline at this
205 location destabilizes the GerS homodimer and promotes GerS monomer formation.
206
207 To test whether the conserved proline in the analogous position of other monomeric PLLLF
208 proteins regulates dimerization, we exchanged *E. coli* LolA Pro65 with a threonine. Remarkably,
209 while wild-type LolA eluted as a monomer, $LolA^{P65T}$ eluted primarily as a dimer (Figure 4C).
210 Taken together, these data highlight how a proline at this site promotes β-turn formation and
211 thus the monomeric form, consistent with past studies of β-turns [55,56].
212
213 While the T72P substitution effectively shifted the dimer-to-monomer equilibrium toward the
214 monomer state, it did not completely prevent the formation of GerS homodimers. To further
215 destabilize the dimer, we introduced a second proline at the fourth residue, creating the hinge
216 sequence Lys71-Pro72-Asp73-Pro74 (KPDP). Since prolines in β-turns are often paired with
217 flexible glycine residues to counteract their rigidity [56–58], we also replaced the first and third
218 residues in the hinge with glycines, yielding a Gly71-Pro72-Gly73-Pro74 (GPGP) hinge
219 sequence. The $GerS^{KPDP}$ variant eluted as a single peak at a volume that falls between the

220 dimer and monomer peaks, suggesting that the variant interconverts between the monomer and
221 dimer forms as it is resolved on the column, whereas the GerS^{GPGP} variant exclusively eluted as
222 a monomer (Figure 4D). These results indicate that the addition of a second proline in the
223 strand-swap hinge further destabilizes the GerS homodimer, i.e., favors the monomeric form,
224 especially when glycines are introduced to provide greater conformation flexibility.
225
226 **Interaction with CwlD requires both strand swapping and a salt bridge.**
227 Since we originally hypothesized that strand-swapping in GerS enhances its ability to bind CwlD
228 based on analyses of other strand-swapped proteins, we next tested if destabilizing the
229 homodimer affects its affinity for CwlD. To this end, we co-affinity purified His$_6$-tagged CwlD with
230 untagged GerS variants and analyzed their interactions by SEC. Untagged GerS^{WT}, GerS^{K71R},
231 and GerS^{N74L} co-purified efficiently with His$_6$-tagged GerS and eluted as the GerS:CwlD
232 complex as well as the GerS and CwlD monomers (Figure 5A, Supplementary Figure 9). It
233 should be noted that the GerS:CwlD complex eluted as several peaks due to the higher
234 resolution SEC performed relative to our prior work. In contrast, considerably less GerS^{D73N} and
235 GerS^{T72P} co-purified with His$_6$-tagged CwlD (Figure 5A, Supplementary Figure 9). While the
236 former result is consistent with GerS^{D73N} being unstable *in vitro*, the decrease in GerS^{T72P} co-
237 purifying with His$_6$-tagged CwlD relative to WT GerS (Fig. 5B) is consistent with the hypothesis
238 that the strand-swapped GerS dimer has a higher affinity for CwlD. The GerS^{KPDP} and GerS^{GPGP}
239 variants exhibited even lower affinity for His$_6$-CwlD, although detectable amounts of GerS^{KPDP}
240 and GerS^{GPGP} were still observed in the co-elution samples (Figure 5B). Together, these data
241 suggest that while destabilization of the GerS homodimer disrupts CwlD interaction, it is
242 insufficient to disrupt the interaction completely.
243
244 Since our prior work revealed that the interaction between GerS and CwlD is partially dependent
245 on a salt bridge that forms between arginine 169 of CwlD and aspartate 106 of GerS [26], we

246 reasoned that GerS binding to CwlD depends on both the salt bridge and GerS strand swap. To
247 test this possibility, we combined the salt-bridge and strand-swapped mutations to generate
248 $GerS^{T72P,D106R}$, $GerS^{KPDP,D106R}$, and $GerS^{GPGP,D106R}$ variants. Remarkably, these combined
249 mutations fully disrupted GerS binding to CwlD, since the untagged GerS variants were not
250 detectable in the co-elutions with His_6-tagged CwlD.
251
252 To determine the impact of the strand-swap and the combined salt-bridge and strand-swap
253 mutations on germination, we complemented our Δ*gerS* mutant with constructs encoding these
254 mutations, purified the resulting spores, and analyzed their germination efficiency using an
255 optical density-based germination assay induced by exposure to 1% taurocholate in BHIS
256 media. By calculating the change in optical density of the spores during germination, we found
257 that none of the strand-swap mutants significantly altered germination relative to WT, consistent
258 with our prior finding that a *gerS D106R* complementation strain exhibits a modest but
259 significant decrease in germination [26]. Remarkably, when the strand-swap and salt-bridge
260 mutations were combined, the *gerS T72P-D106R*, *gerS KPDP-D106R*, and *gerS GPGP-D106R*
261 complementation strains phenocopied their parental Δ*gerS* strain in failing to germinate. It
262 should be noted that the GPGP substitutions significantly decreased the stability of GerS in *C.*
263 *difficile* sporulating cells because GerS levels were greatly reduced in *gerS GPGP*
264 (Supplementary Figure 10). Combining the salt-bridge mutations with the strand-swap mutations
265 further destabilized GerS levels in sporulating cells (Supplementary Figure 10), consistent with
266 their greatly reduced affinity for CwlD (Figure 5). Taken together, our data highlight the
267 importance of both the strand swap and salt bridge on GerS binding to CwlD and, by extension,
268 regulation of *C. difficile* spore germination.
269
270
271

272 **Discussion**

273

274 Our prior discovery that the *C. difficile* GerS lipoprotein binds the CwlD amidase as a strand-
275 swapped dimer led to the question of whether strand-swapping by GerS enhances its ability to
276 allosterically activate the CwlD amidase [26]. By identifying mutations that shift the GerS
277 dimer:monomer equilibrium to the monomeric form (Figure 3), we showed that monomeric GerS
278 has greatly reduced affinity for its binding partner, CwlD, which in turn reduces, but does not
279 abolish, *C. difficile* spore germination (Figure 5). Since combining monomer-promoting
280 mutations with a salt-bridge substitution that disrupts a GerS:CwlD binding interface abrogates
281 GerS's ability to activate the CwlD amidase, our data highlight the critical importance of GerS's
282 hinge region in regulating the allosteric activation of CwlD.

283

284 While our findings are consistent with prior work highlighting that strand-swapping can stabilize
285 adhesive interactions, such as in cadherins and the LolA^{F68E} variant, they also raise the
286 possibility that the dynamic instability of the strand-swapped dimer, which exists in near-equal
287 proportions with the monomeric form *in vitro* (Figure 3), contributes to GerS function. Strand
288 swapping is sometimes the result of localized unfolding around the hinge. While the rest of the
289 protein folds, the strand to be swapped unfolds, leading to monomeric and dimeric
290 conformations [27,59]. Like GerS, the yeast cell-cycle regulation protein p13suc1 has both a
291 native monomer and dimer state [35]. Two prolines in the hinge generate tension in each state,
292 functioning as a sort of spring between both a monomer and dimer conformation. Shifts toward
293 either dimer or monomer populations are observed by substitutions in the hinge of the swapped
294 structure. In a similar way, K71R and N74L substitutions may stabilize the dimeric conformation,
295 while T72P, KPDP, and GPGP substitutions stabilize folding of the monomeric conformation.
296 The persistence of the two stable populations in near equal proportions suggests that the GerS
297 monomer may be functionally important, perhaps to ensure that GerS transiently interacts with

298 CwlD during MAL formation. Alternatively, there may be additional players that stabilize one
299 conformation over another during the regulation of MAL formation.
300
301 Our finding that a single substitution of threonine for proline in the hinge region dramatically
302 alters the conformational stability of GerS implies that PLLLF proteins have evolved an inherent
303 instability at this specific site, which may serve as a foundation for their structural flexibility. The
304 last common ancestor of *C. difficile* and *E. coli* lived billions of years ago. However, a single
305 reciprocal substitution at this site in LolA ($LolA^{P65T}$) is enough to shift its structure from a
306 monomer to a homodimer (Figure 4). This evidence, along with the similarly strand-swapped
307 $LolA^{F68E}$ (published F47E) [37,38] structure, support the idea that the LolA monomeric structure
308 around these sites is intrinsically unstable. These findings also highlight the ease with which
309 PLLLF proteins can evolve strand-swapped dimerization. This finding also raises the possibility
310 of a shared ancestry between LolA and GerS. During the evolution of monoderm bacteria, which
311 involved the loss of the ancestral outer membrane [60–62], there would no longer be a need to
312 transport lipoproteins across the periplasmic space, facilitating a specialization of the ancestral
313 proteins during sporulation in endospore-forming monoderms [13,26]. This hypothesis may also
314 clarify why PLLLF proteins are absent in certain non-spore-forming monoderms such as
315 *Staphylococcus aureus* and the seemingly convergent roles of LppX [10] and Lpr proteins
316 [11,12] in transporting glycolipids across the mycobacterial periplasm.
317
318 Much work remains to be done to understand precisely why GerS strand swapping stabilizes its
319 interaction with CwlD. Notably, CwlD binding to its Zn^{2+} co-factor also stabilizes the GerS:CwlD
320 interaction, so it is possible that Zn^{2+}-bound CwlD adopts a conformation that similarly promotes
321 GerS strand-swapping. Identifying the allosteric circuit that allows GerS binding to CwlD to be
322 communicated to CwlD's active site and vice versa will likely provide insight into the role of
323 GerS strand-swapping in the allosteric activation of CwlD. Another question that arises from our

324 identification of GerS orthologs in other clostridial species that do not form dimers is whether
325 these GerS orthologs have additional or different conserved functions beyond regulating CwlD
326 activity during cortex modification? The requirement of CwlD for GerS processing and
327 incorporation into the spore may indicate that GerS functions in a very specialized way in the
328 Peptostreptococcaceae family[25]. In contrast, it possible that GerS orthologs in other
329 Clostridia, function similarly to SsdC in *B. subtilis*, which is thought to act as a conduit between
330 spore coat synthesis and cortex modification [13]. Nevertheless, how these orthologs are
331 incorporated into the spore if they do not interact with CwlD as well as whether GerS and CwlD
332 can independently localize to the forespore remain open questions and will requiring further
333 investigation beyond studies in *C. difficile*.
334
335
336 **Materials and Methods**
337
338 **Bacterial strains and growth conditions.** *C. difficile* strain construction was performed using
339 630Δ*erm*Δ*cwlD*Δ*pyrE* and 630Δ*erm*Δ*gerS*Δ*pyrE* as the parental strains via *pyrE*-based allelic-
340 coupled exchange (ACE). This system allows for single-copy complementation of the Δ*cwlD* and
341 Δ*gerS* parental mutants, from an ectopic locus. The *C. difficile* strains used are listed in Table S1.
342 They were grown on brain heart infusion media (BHIS) supplemented with taurocholate (TA, 0.1%
343 wt/vol; 1.9 mM), thiamphenicol (10-15 µg /mL), kanamycin (50 µg/ml), cefoxitin (8 µg/ml) and L-
344 cysteine (0.1% w/v; 8.25 mM) as needed. For ACE, *C. difficile* defined medium (CDDM) was
345 supplemented with 5-fluoroorotic acid (5-FOA) at 2 mg/ml and uracil at 5 µg/ml. Cultures were
346 grown at 37°C under anaerobic conditions using a gas mixture containing 85% N_2, 5% CO_2 and
347 10% H_2.
348 The *Escherichia coli* strains used for BL21(DE3)-based protein production and for
349 HB101/pRK24-based conjugations are listed in Table S1. *E. coli* strains were grown at 37°C with

350 shaking at 225 rpm in Luria-Bertani broth (LB). The media was supplemented with
351 chloramphenicol (20 µg/ml), ampicillin (50 µg/ml), or kanamycin (30 µg/ml) as indicated.

352 ***E. coli* strain construction.** Plasmid constructs were confirmed by sequencing using Genewiz
353 or Plasmidsaurus and transformed into either the HB101/pRK24 conjugation strain (used with *C.*
354 *difficile*) or BL21(DE3) expression strain.

355 ***C. difficile* strain construction and complementation**. Allele-couple exchange (ACE) was used
356 to construct all complementation strains as previously described by conjugating HB101/ pRK24
357 carrying pMTL-YN1C plasmids into Δ*pyrE*-based strains.
358

359 **Protein purification.** Starter cultures were grown in 20 mL LB broth with 100 µg/mL ampicillin
360 and, in some cases, 30 µg/mL of kanamycin. Terrific broth (TB) with ampicillin and kanamycin
361 was inoculated with the starter culture (1:1000) and incubated for ~60 hr at 20°C with 225 rpm
362 shaking. The purifications were carried out in two steps: nickel bead-based affinity purification
363 followed by size exclusion chromatography (SEC). Affinity purification was carried out as stated
364 above: the cells were pelleted, resuspended in lysis buffer (500 mM NaCl, 50 mM Tris [pH 7.5],
365 15 mM imidazole, 10% [vol/vol] glycerol, 2 mM ß-mercaptoethanol), flash frozen in liquid
366 nitrogen, thawed and then sonicated. The insoluble material was pelleted and the soluble
367 fraction was incubated with Ni-NTA agarose beads (Qiagen) for 2 hours to capture the His_6
368 tagged proteins. Washes were carried out three times with low imidazole buffer (500mM NaCl,
369 10mM Tris-HCl pH 7.5, 10% (v/v) glycerol, 15 mM imidazole, 2 mM ß -mercaptoethanol) to
370 decrease non-specific binding to the beads. Proteins were eluted using high-imidazole buffer
371 (500 mM NaCl, 50 mM Tris [pH 7.5], 200 mM imidazole, 10% [vol/vol] glycerol, 2 mM ß-
372 mercaptoethanol) after nutating the sample for 5 to 10 min. Pooled protein elutions were
373 concentrated to 20 mg/ml or less in a gel filtration buffer consisting of 200 mM NaCl, 10 mM Tris
374 HCl pH 7.5, 5% glycerol, and 1 mM DTT. SEC was carried out using a Superdex 200 Increase

375 10/300 GL (GE Healthcare) column. Proteins were resolved on 14% SDS-PAGE gels, and the
376 gels were stained using GelCode Blue according to the manufacturer's
377 instructions (ThermoFisher Scientific). The purified proteins were concentrated, aliquoted, flash
378 frozen, and stored at - 20℃ for future analysis.
379

380 **Plate-based sporulation assays.** *C. difficile* strains were inoculated from glycerol stocks
381 overnight onto BHIS plates containing taurocholate. Colonies arising from these plates were used
382 to inoculate liquid BHIS cultures, which were grown to early stationary phase, back-diluted 1:50
383 into BHIS, and grown until the cultures reached an OD_{600} between 0.35 and 0.75. Sporulation was
384 by spotting 120 µL of the exponential cultures onto 70:30 media after which cells were analyzed
385 by phase-contrast microscopy and harvested for western blot analyses at 15-22 hrs)..
386

387 **Western blot analysis.** Samples for immunoblotting were prepared by resuspending sporulating
388 cell pellets in 100 µl of PBS, and freeze-thawing a 50 µL aliquot of this resuspension for three
389 cycles. The pellet was then resuspended in 100 µl EBB buffer (8 M urea, 2 M thiourea, 4% [wt/vol]
390 SDS, 2% [vol/vol] ß-mercaptoethanol). *C. difficile* spores (~1 x 10^6) were resuspended in EBB
391 buffer, which can extract proteins in all layers of the spore, including the core. Both sporulating
392 cells and spores were incubated at 95°C for 20 min with vortex mixing. Samples were centrifuged
393 for 5 min at 15,000 rpm, and 4 x sample buffer (40% [vol/vol] glycerol, 1 M Tris [pH 6.8], 20%
394 [vol/vol] ß -mercaptoethanol, 8% [wt/vol] SDS, 0.04% [wt/vol] bromophenol blue) was added.
395 Samples were incubated again at 95°C for 5 to 10 min with vortex mixing followed by
396 centrifugation for 5 min at 15,000 rpm. The samples were resolved by the use of 14% SDS-PAGE
397 gels and transferred to a Millipore Immobilon-FL polyvinylidene difluoride (PVDF) membrane. The
398 membranes were blocked in Odyssey blocking buffer with 0.1% (vol/vol) Tween 20. Polyclonal
399 rabbit anti-GerS and anti-CwlD antibodies were used at a 1:500 dilution. Polyclonal mouse anti-

400 SpoIVA and mouse anti-SleC antibodies were used at 1:2,500 dilution and 1:5,000 dilution,
401 respectively. IRDye 680CW and 800CW infrared dye-conjugated secondary antibodies were used
402 at 1:25,000 dilutions. An odyssey LiCor CLx was used to visualize secondary antibody infrared
403 fluorescence emissions.
404
405 **Spore purification.** Sporulation was induced on 70:30 agar plates for 3-5 days and the cultures
406 were harvested for spore purifications. Spores were washed 6 times in ice-cold water, incubated
407 overnight in water on ice, treated with DNase I (New England Biolabs) at 37°C for 60 min, and
408 purified on a HistoDenz (Sigma- Aldrich) gradient. Phase-contrast microscopy was used to assess
409 spore purity (>95% pure); the optical density of the spore stock was measured at OD_{600}; and
410 spores were stored in water at 4°C. Two 70:30 plates were used to induce sporulation for each
411 strain; purified spores were resuspended in 200 µl, and the total optical density of this mixture
412 was determined for each strain. At least three independent spore preparations were performed.
413
414 **Germination assay.** Germination assays were performed as previously described (12).
415 Approximately 1 x 10^7 (OD_{600} of 0.35) were resuspended in 100 µl of water, and 10 µl of this
416 mixture was removed for 10-fold serial dilutions in PBS. The dilutions were plated on BHIS-TA,
417 and colonies arising from germinated spores were enumerated at 20 h. Germination efficiencies
418 were calculated by averaging the CFU produced by spores for a given strain relative to the number
419 produced by wild-type spores for at least three biological replicates from two independent spore
420 preparations. Statistical significance was determined by performing a one-way analysis of
421 variance (ANOVA) on natural log-transformed data using Tukey's test.

422 **Germination OD_{600} kinetics assay and phase-contrast microscopy.** For OD_{600}-based kinetic
423 assays with taurocholate in 96-well plates, ~1.6 x 10^7 spores (0.55 OD600 units) for each
424 condition tested were resuspended in BHIS and 180 µL were aliquoted into two wells of a 96 well

425 flat bottom tissue culture plate (Falcon) for each condition tested. The spores were exposed to
426 1% taurocholate, or water (untreated) in a final volume of 200 µL. The OD_{600} of the samples was
427 measured every 3 minutes in a Synergy H1 microplate reader (Biotek) at 37℃ with constant
428 shaking between readings. The change in OD_{600} over time was calculated as the ratio of the
429 OD_{600} at each time point to the OD_{600} at time zero. These assays were performed on three
430 independent spore preparations. Data shown are averages from three replicates.
431 For phase contrast microscopy, purified spores were resuspended to an OD_{600} of 0.5 in BHIS ±
432 1% taurocholate and incubated aerobically for 90 min at 37°C. Samples were spun down (5,000
433 x g, 10 min, 4°C), washed with PBS, and fixed with 3.7% paraformaldehyde for 15 min at RT.
434 Following fixation, samples were washed with PBS and mounted on agarose pads.
435
436
437 **References**

438 [1] A. De Las Peñas, L. Connolly, C.A. Gross, The σE-mediated response to
439 extracytoplasmic stress in *Escherichia coli* is transduced by RseA and RseB, two
440 negative regulators of σE, Mol Microbiol 24 (1997) 373–385.
441 https://doi.org/10.1046/J.1365-2958.1997.3611718.X.

442 [2] M.J. Schurr, H. Yu, J.M. Martinez-Salazar, J.C. Boucher, V. Deretic, Control of AlgU, a
443 member of the sigma E-like family of stress sigma factors, by the negative regulators
444 MucA and MucB and *Pseudomonas aeruginosa* conversion to mucoidy in cystic fibrosis,
445 J Bacteriol 178 (1996) 4997–5004. https://doi.org/10.1128/JB.178.16.4997-5004.1996.

446 [3] D. Jaiman, R. Nagampalli, K. Persson, A comparative analysis of lipoprotein transport
447 proteins: LolA and LolB from *Vibrio cholerae* and LolA from *Porphyromonas gingivalis*,
448 Scientific Reports 2023 13:1 13 (2023) 1–10. https://doi.org/10.1038/s41598-023-33705-
449 y.

450 [4] S. Okuda, H. Tokuda, Model of mouth-to-mouth transfer of bacterial lipoproteins through
451 inner membrane LolC, periplasmic LolA, and outer membrane LolB, Proc Natl Acad Sci U
452 S A 106 (2009) 5877–5882.
453 https://doi.org/10.1073/PNAS.0900896106/SUPPL_FILE/0900896106SI.PDF.

454 [5] V. Furlanetto, C. Divne, LolA and LolB from the plant-pathogen *Xanthomonas campestris*
455 forms a stable heterodimeric complex in the absence of lipoprotein, Front Microbiol 14
456 (2023) 1216799. https://doi.org/10.3389/FMICB.2023.1216799/BIBTEX.

[6] K.L. May, M. Grabowicz, Outer membrane lipoproteins: late to the party, but the center of attention, J Bacteriol (2024). https://doi.org/10.1128/JB.00442-24.

[7] E.D. LoVullo, L.F. Wright, V. Isabella, J.F. Huntley, M.S. Pavelka, Revisiting the gram-negative lipoprotein paradigm, J Bacteriol 197 (2015) 1705–1715. https://doi.org/10.1128/JB.02414-14/SUPPL_FILE/ZJB999093599SO4.XLSX.

[8] S. ichiro Narita, H. Tokuda, Sorting of bacterial lipoproteins to the outer membrane by the Lol system, Methods Mol Biol 619 (2010) 117–129. https://doi.org/10.1007/978-1-60327-412-8_7.

[9] S.Y. Tanaka, S.I. Narita, H. Tokuda, Characterization of the *Pseudomonas aeruginosa* Lol system as a lipoprotein sorting mechanism, Journal of Biological Chemistry 282 (2007) 13379–13384. https://doi.org/10.1074/jbc.M611840200.

[10] G. Sulzenbacher, S. Canaan, Y. Bordat, O. Neyrolles, G. Stadthagen, V. Roig-Zamboni, J. Rauzier, D. Maurin, F. Laval, M. Daffé, C. Cambillau, B. Gicquel, Y. Bourne, M. Jackson, LppX is a lipoprotein required for the translocation of phthiocerol dimycocerosates to the surface of *Mycobacterium tuberculosis*, EMBO Journal 25 (2006) 1436–1444. https://doi.org/10.1038/SJ.EMBOJ.7601048/SUPPL_FILE/EMBJ7601048-SUP-0001.PDF.

[11] M.G. Drage, H.C. Tsai, N.D. Pecora, T.Y. Cheng, A.R. Arida, S. Shukla, R.E. Rojas, C. Seshadri, D.B. Moody, W.H. Boom, J.C. Sacchettini, C. V. Harding, *Mycobacterium tuberculosis* lipoprotein LprG (Rv1411c) binds triacylated glycolipid agonists of Toll-like receptor 2, Nature Structural & Molecular Biology 2010 17:9 17 (2010) 1088–1095. https://doi.org/10.1038/nsmb.1869.

[12] J.S. Kim, L. Jiao, J. Il Oh, N.C. Ha, Y.H. Kim, Crystal structure and functional implications of LprF from *Mycobacterium tuberculosis* and *M. bovis*, Acta Crystallogr D Biol Crystallogr 70 (2014) 2619–2630. https://doi.org/10.1107/S1399004714016599.

[13] J. Luhur, H. Chan, B. Kachappilly, A. Mohamed, C. Morlot, M. Awad, D. Lyras, N. Taib, S. Gribaldo, D.Z. Rudner, C.D.A. Rodrigues, A dynamic, ring-forming MucB / RseB-like protein influences spore shape in *Bacillus subtilis*, PLoS Genet 16 (2020) e1009246. https://doi.org/10.1371/JOURNAL.PGEN.1009246.

[14] K.A. Fimlaid, O. Jensen, M.L. Donnelly, M.B. Francis, J.A. Sorg, A. Shen, Identification of a Novel Lipoprotein Regulator of *Clostridium difficile* Spore Germination, PLoS Pathog 11 (2015) e1005239. https://doi.org/10.1371/JOURNAL.PPAT.1005239.

[15] D.A. Burns, J.T. Heap, N.P. Minton, SleC is essential for germination of *Clostridium difficile* spores in nutrient-rich medium supplemented with the bile salt taurocholate, J Bacteriol 192 (2010) 657–664. https://doi.org/10.1128/JB.01209-09/ASSET/F0B6A88D-0D10-4FE5-ADDE-C2E652FF1E28/ASSETS/GRAPHIC/ZJB9990993070005.JPEG.

[16] D. Paredes-Sabja, P. Setlow, M.R. Sarker, SleC Is Essential for Cortex Peptidoglycan Hydrolysis during Germination of Spores of the Pathogenic Bacterium *Clostridium perfringens*, J Bacteriol 191 (2009) 2711–2720. https://doi.org/10.1128/JB.01832-08.

496 [17] C.M. Adams, B.E. Eckenroth, E.E. Putnam, S. Doublié, A. Shen, Structural and
497 Functional Analysis of the CspB Protease Required for *Clostridium* Spore Germination,
498 PLoS Pathog 9 (2013) e1003165. https://doi.org/10.1371/JOURNAL.PPAT.1003165.

499 [18] S. Okamura, K. Urakami, M. Kimata, T. Aoshima, S. Shimamoto, R. Moriyama, S.
500 Makino, The N-terminal prepeptide is required for the production of spore cortex-lytic
501 enzyme from its inactive precursor during germination of *Clostridium perfringens* S40
502 spores, Mol Microbiol 37 (2000) 821–827. https://doi.org/10.1046/J.1365-
503 2958.2000.02047.X.

504 [19] K. Urakami, S. Miyata, R. Moriyama, K. Sugimoto, S. Makino, Germination-specific
505 cortex-lytic enzymes from *Clostridium perfringens* S40 spores: time of synthesis,
506 precursor structure and regulation of enzymatic activity, FEMS Microbiol Lett 173 (1999)
507 467–473. https://doi.org/10.1111/J.1574-6968.1999.TB13540.X.

508 [20] D. Gutelius, K. Hokeness, S.M. Logan, C.W. Reid, Functional analysis of SleC from
509 *Clostridium difficile*: an essential lytic transglycosylase involved in spore germination,
510 Microbiology (N Y) 160 (2014) 209. https://doi.org/10.1099/MIC.0.072454-0.

511 [21] T. Fukushima, H. Yamamoto, A. Atrih, S.J. Foster, J. Sekiguchi, A polysaccharide
512 deacetylase gene (pdaA) is required for germination and for production of muramic δ-
513 lactam residues in the spore cortex of *Bacillus subtilis*, J Bacteriol 184 (2002) 6007–6015.
514 https://doi.org/10.1128/JB.184.21.6007-6015.2002/ASSET/281D2E2F-2AB6-4943-9460-
515 50EB1BA91E0B/ASSETS/GRAPHIC/JB2120422006.JPEG.

516 [22] H. Coullon, A. Rifflet, R. Wheeler, C. Janoir, I.G. Boneca, T. Candela, N-Deacetylases
517 required for muramic-lactam production are involved in *Clostridium difficile* sporulation,
518 germination, and heat resistance, Journal of Biological Chemistry 293 (2018) 18040–
519 18054. https://doi.org/10.1074/JBC.RA118.004273/ATTACHMENT/A0930DBF-1D55-
520 4CDE-96DE-AEFCB897DBF5/MMC1.ZIP.

521 [23] M.J. Tobin, S.Y. Cho, W. Profy, T.M. Ryan, D.H. Le, C. Lin, E.Z. Yip, J.L. Dorsey, B.R.
522 Levy, J.D. Rhodes, M.A. Welsh, Reconstituting Spore Cortex Peptidoglycan Biosynthesis
523 Reveals a Deacetylase That Catalyzes Transamidation, (2023).
524 https://doi.org/10.1021/acs.biochem.3c00100.

525 [24] C. Kim, M. Lee, B.T. Birhanu, D. Hesek, M. Chang, S. Mobashery, Synthesis of Muramyl-
526 δ-Lactam in Spore Peptidoglycan of *Clostridioides difficile*, ChemBioChem 24 (2023)
527 e202300282. https://doi.org/10.1002/CBIC.202300282.

528 [25] O.R. Diaz, C. V. Sayer, D.L. Popham, A. Shen, *Clostridium difficile* Lipoprotein GerS Is
529 Required for Cortex Modification and Thus Spore Germination, MSphere 3 (2018).
530 https://doi.org/10.1128/MSPHERE.00205-18/SUPPL_FILE/SPH003182575SF7.TIF.

531 [26] C.A. Feliciano, B.E. Eckenroth, O.R. Diaz, S. Doublié, A. Shen, A lipoprotein allosterically
532 activates the CwlD amidase during *Clostridioides difficile* spore formation, PLoS Genet 17
533 (2021) e1009791. https://doi.org/10.1371/JOURNAL.PGEN.1009791.

534 [27] N.M. Mascarenhas, S. Gosavi, Understanding protein domain-swapping using structure-
535 based models of protein folding, Prog Biophys Mol Biol 128 (2016) 113.
536 https://doi.org/10.1016/J.PBIOMOLBIO.2016.09.013.

537 [28] M.J. Bennett, D. Eisenberg, Refined structure of monomelic diphtheria toxin at 2.3 Å
538 resolution, Protein Science 3 (1994) 1464–1475.
539 https://doi.org/10.1002/PRO.5560030912.

540 [29] S.F. Carroll, J.T. Barbieri, R.J. Collier, Dimeric Form of Diphtheria Toxin: Purification and
541 Characterization, Biochemistry 25 (1986) 2425–2430.
542 https://doi.org/10.1021/BI00357A019.

543 [30] P.R. Gouldson, C.R. Snell, R.P. Bywater, C. Higgs, C.A. Reynolds, Domain swapping in
544 G-protein coupled receptor dimers., Protein Engineering, Design and Selection 11 (1998)
545 1181–1193. https://doi.org/10.1093/PROTEIN/11.12.1181.

546 [31] L. Vitagliano, S. Adinolfi, F. Sica, A. Merlino, A. Zagari, L. Mazzarella, A potential
547 allosteric subsite generated by domain swapping in bovine seminal ribonuclease, J Mol
548 Biol 293 (1999) 569–577. https://doi.org/10.1006/JMBI.1999.3158.

549 [32] R. Janowski, M. Kozak, E. Jankowska, Z. Grzonka, A. Grubb, M. Abrahamson, M.
550 Jaskolski, Human cystatin C, an amyloidogenic protein, dimerizes through three-
551 dimensional domain swapping, Nature Structural Biology 2001 8:4 8 (2001) 316–320.
552 https://doi.org/10.1038/86188.

553 [33] A.D. Cameron, B. Olin, M. Ridderström, B. Mannervik, T.A. Jones, Crystal structure of
554 human glyoxalase I—evidence for gene duplication and 3D domain swapping, EMBO J
555 16 (1997) 3386–3395. https://doi.org/10.1093/EMBOJ/16.12.3386.

556 [34] J. Vendome, S. Posy, X. Jin, F. Bahna, G. Ahlsen, L. Shapiro, B. Honig, Molecular design
557 principles underlying β-strand swapping in the adhesive dimerization of cadherins, Nature
558 Structural & Molecular Biology 2011 18:6 18 (2011) 693–700.
559 https://doi.org/10.1038/nsmb.2051.

560 [35] F. Rousseau, J.W.H. Schymkowitz, H.R. Wilkinson, L.S. Itzhaki, Three-dimensional
561 domain swapping in p13suc1 occurs in the unfolded state and is controlled by conserved
562 proline residues, Proceedings of the National Academy of Sciences 98 (2001) 5596–
563 5601. https://doi.org/10.1073/PNAS.101542098.

564 [36] K. Shivaji Paithankar, M. Enderle, D.C. Wirthensohn, A. Miller, M. Schlesner, F. Pfeiffer,
565 A. Rittner, M. Grininger, D. Oesterhelt, Structure of the archaeal chemotaxis protein CheY
566 in a domain-swapped dimeric conformation, (n.d.).
567 https://doi.org/10.1107/S2053230X19010896.

568 [37] A. Miyamoto, S. ichi Matsuyama, H. Tokuda, Dominant negative mutant of a lipoprotein-
569 specific molecular chaperone, LolA, tightly associates with LolCDE, FEBS Lett 528
570 (2002) 193–196. https://doi.org/10.1016/S0014-5793(02)03305-7.

571 [38] E. Kaplan, N.P. Greene, A. Crow, V. Koronakis, Insights into bacterial lipoprotein
572 trafficking from a structure of LolA bound to the LolC periplasmic domain, Proc Natl Acad
573 Sci U S A 115 (2018) E7389–E7397.
574 https://doi.org/10.1073/PNAS.1806822115/SUPPL_FILE/PNAS.1806822115.SM03.MOV.

575 [39] M. van Kempen, S.S. Kim, C. Tumescheit, M. Mirdita, J. Lee, C.L.M. Gilchrist, J. Söding,
576 M. Steinegger, Fast and accurate protein structure search with Foldseek, Nature

Biotechnology 2023 42:2 42 (2023) 243–246. https://doi.org/10.1038/s41587-023-01773-0.

[40] M. Blum, A. Andreeva, L. Cavalcanti Florentino, S. Rocio Chuguransky, T. Grego, E. Hobbs, B. Lazaro Pinto, A. Orr, T. Pa ysan-Laf osse, I. Ponamareva, G.A. Salazar, N. Bordin, P. eer Bor, A. Br idg, L. Colw ell, J. Gough, D.H. Haft, I. Letunic, F. Llinares-López, A. Marchler-Bauer, L. Meng-Papaxanthos, H. Mi, D.A. Natale, C.A. Orengo, A.P. Pandur ang an, D. Pio esan, C. ine Rivoire, C.J. istian Sigr ist, N. mada Thanki, F. ançoise Thibaud-Nissen, P.D. Thomas, S.C. Tosatto, C.H. W, A. Bat eman, InterPro: the protein sequence classification resource in 2025, Nucleic Acids Res 1 (2013) 13–14. https://doi.org/10.1093/NAR/GKAE1082.

[41] C. Camacho, G. Coulouris, V. Avagyan, N. Ma, J. Papadopoulos, K. Bealer, T.L. Madden, BLAST+: Architecture and applications, BMC Bioinformatics 10 (2009) 1–9. https://doi.org/10.1186/1471-2105-10-421/FIGURES/4.

[42] S.F. Altschul, W. Gish, W. Miller, E.W. Myers, D.J. Lipman, Basic local alignment search tool, J Mol Biol 215 (1990) 403–410. https://doi.org/10.1016/S0022-2836(05)80360-2.

[43] L. Holm, A. Laiho, P. Törönen, M. Salgado, DALI shines a light on remote homologs: One hundred discoveries, Protein Science 32 (2023) e4519. https://doi.org/10.1002/PRO.4519.

[44] J. Abramson, J. Adler, J. Dunger, R. Evans, T. Green, A. Pritzel, O. Ronneberger, L. Willmore, A.J. Ballard, J. Bambrick, S.W. Bodenstein, D.A. Evans, C.C. Hung, M. O'Neill, D. Reiman, K. Tunyasuvunakool, Z. Wu, A. Žemgulytė, E. Arvaniti, C. Beattie, O. Bertolli, A. Bridgland, A. Cherepanov, M. Congreve, A.I. Cowen-Rivers, A. Cowie, M. Figurnov, F.B. Fuchs, H. Gladman, R. Jain, Y.A. Khan, C.M.R. Low, K. Perlin, A. Potapenko, P. Savy, S. Singh, A. Stecula, A. Thillaisundaram, C. Tong, S. Yakneen, E.D. Zhong, M. Zielinski, A. Žídek, V. Bapst, P. Kohli, M. Jaderberg, D. Hassabis, J.M. Jumper, Accurate structure prediction of biomolecular interactions with AlphaFold 3, Nature 2024 630:8016 630 (2024) 493–500. https://doi.org/10.1038/s41586-024-07487-w.

[45] E.C. Meng, T.D. Goddard, E.F. Pettersen, G.S. Couch, Z.J. Pearson, J.H. Morris, T.E. Ferrin, UCSF ChimeraX: Tools for structure building and analysis, Protein Science 32 (2023) e4792. https://doi.org/10.1002/PRO.4792.

[46] K. Remans, K. Pauwels, P. van Ulsen, L. Buts, P. Cornelis, J. Tommassen, S.N. Savvides, K. Decanniere, P. Van Gelder, Hydrophobic Surface Patches on LolA of *Pseudomonas aeruginosa* Are Essential for Lipoprotein Binding, J Mol Biol 401 (2010) 921–930. https://doi.org/10.1016/J.JMB.2010.06.067.

[47] K. Takeda, H. Miyatake, N. Yokota, S.I. Matsuyama, H. Tokuda, K. Miki, Crystal structures of bacterial lipoprotein localization factors, LolA and LolB, EMBO J 22 (2003) 3199–3209. https://doi.org/10.1093/EMBOJ/CDG324.

[48] J. Botas, Á. Rodríguez Del Río, J. Giner-Lamia, J. Huerta-Cepas, GeCoViz: genomic context visualisation of prokaryotic genes from a functional and evolutionary perspective, Nucleic Acids Res 50 (2022) W352–W357. https://doi.org/10.1093/NAR/GKAC367.

[49] J. Herson, M. Krummenacker, A. Spaulding, P. O'Maille, P.D. Karp, The Genome Explorer genome browser, MSystems 9 (2024). https://doi.org/10.1128/MSYSTEMS.00267-24/ASSET/D092CD98-EDF4-4F91-B5B5-0333B26B6D93/ASSETS/IMAGES/LARGE/MSYSTEMS.00267-24.F007.JPG.

[50] J.W. O'Neill, D.E. Kim, K. Johnsen, D. Baker, K.Y.J. Zhang, Single-site mutations induce 3D domain swapping in the B1 domain of Protein L from *Peptostreptococcus magnus*, Structure 9 (2001) 1017–1027. https://doi.org/10.1016/S0969-2126(01)00667-0/ASSET/72670EC8-3DCE-47A6-B0BE-0F27AFC6C8EF/MAIN.ASSETS/FX3.JPG.

[51] K.H. Miller, J.R. Karr, S. Marqusee, A Hinge Region cis-Proline in Ribonuclease A Acts as a Conformational Gatekeeper for C-Terminal Domain Swapping, J Mol Biol 400 (2010) 567–578. https://doi.org/10.1016/J.JMB.2010.05.017.

[52] M. Orlikowska, E. Jankowska, R. Kołodziejczyk, M. Jaskólski, A. Szymańska, Hinge-loop mutation can be used to control 3D domain swapping and amyloidogenesis of human cystatin C, J Struct Biol 173 (2011) 406–413. https://doi.org/10.1016/J.JSB.2010.11.009.

[53] A. Shen, P.J. Lupardus, M. Morell, E.L. Ponder, A.M. Sadaghiani, K.C. Garcia, M. Bogyo, Simplified, Enhanced Protein Purification Using an Inducible, Autoprocessing Enzyme Tag, PLoS One 4 (2009) e8119. https://doi.org/10.1371/JOURNAL.PONE.0008119.

[54] A. Chikunova, M.P. Manley, C.N. Heijjer, C.S. Drenth, A.J. Cramer-Blok, M.U.D. Ahmad, A. Perrakis, M. Ubbink, Conserved proline residues prevent dimerization and aggregation in the β-lactamase BlaC, Protein Science 33 (2024) e4972. https://doi.org/10.1002/PRO.4972.

[55] H. Fu, G.R. Grimsley, A. Razvi, J.M. Scholtz, C.N. Pace, Increasing protein stability by improving beta-turns, Proteins: Structure, Function, and Bioinformatics 77 (2009) 491–498. https://doi.org/10.1002/PROT.22509.

[56] C.M. Wilmot, J.M. Thornton, Analysis and prediction of the different types of β-turn in proteins, J Mol Biol 203 (1988) 221–232. https://doi.org/10.1016/0022-2836(88)90103-9.

[57] E.G. Hutchinson, J.M. Thornton, A revised set of potentials for β-turn formation in proteins, Protein Science 3 (1994) 2207–2216. https://doi.org/10.1002/PRO.5560031206.

[58] M.W. MacArthur, J.M. Thornton, Influence of proline residues on protein conformation, J Mol Biol 218 (1991) 397–412. https://doi.org/10.1016/0022-2836(91)90721-H.

[59] F. Ding, K.C. Prutzman, S.L. Campbell, N. V. Dokholyan, Topological determinants of protein domain swapping, Structure 14 (2006) 5–14. https://doi.org/10.1016/J.STR.2005.09.008.

[60] D. Megrian, N. Taib, J. Witwinowski, C. Beloin, S. Gribaldo, One or two membranes? Diderm Firmicutes challenge the Gram-positive/Gram-negative divide, Mol Microbiol 113 (2020) 659–671. https://doi.org/10.1111/MMI.14469.

[61] N. Taib, D. Megrian, J. Witwinowski, P. Adam, D. Poppleton, G. Borrel, C. Beloin, S. Gribaldo, Genome-wide analysis of the Firmicutes illuminates the diderm/monoderm transition, Nature Ecology & Evolution 2020 4:12 4 (2020) 1661–1672. https://doi.org/10.1038/s41559-020-01299-7.

[62] J. Witwinowski, A. Sartori-Rupp, N. Taib, N. Pende, T.N. Tham, D. Poppleton, J.M. Ghigo, C. Beloin, S. Gribaldo, An ancient divide in outer membrane tethering systems in bacteria suggests a mechanism for the diderm-to-monoderm transition, Nature Microbiology 2022 7:3 7 (2022) 411–422. https://doi.org/10.1038/s41564-022-01066-3.

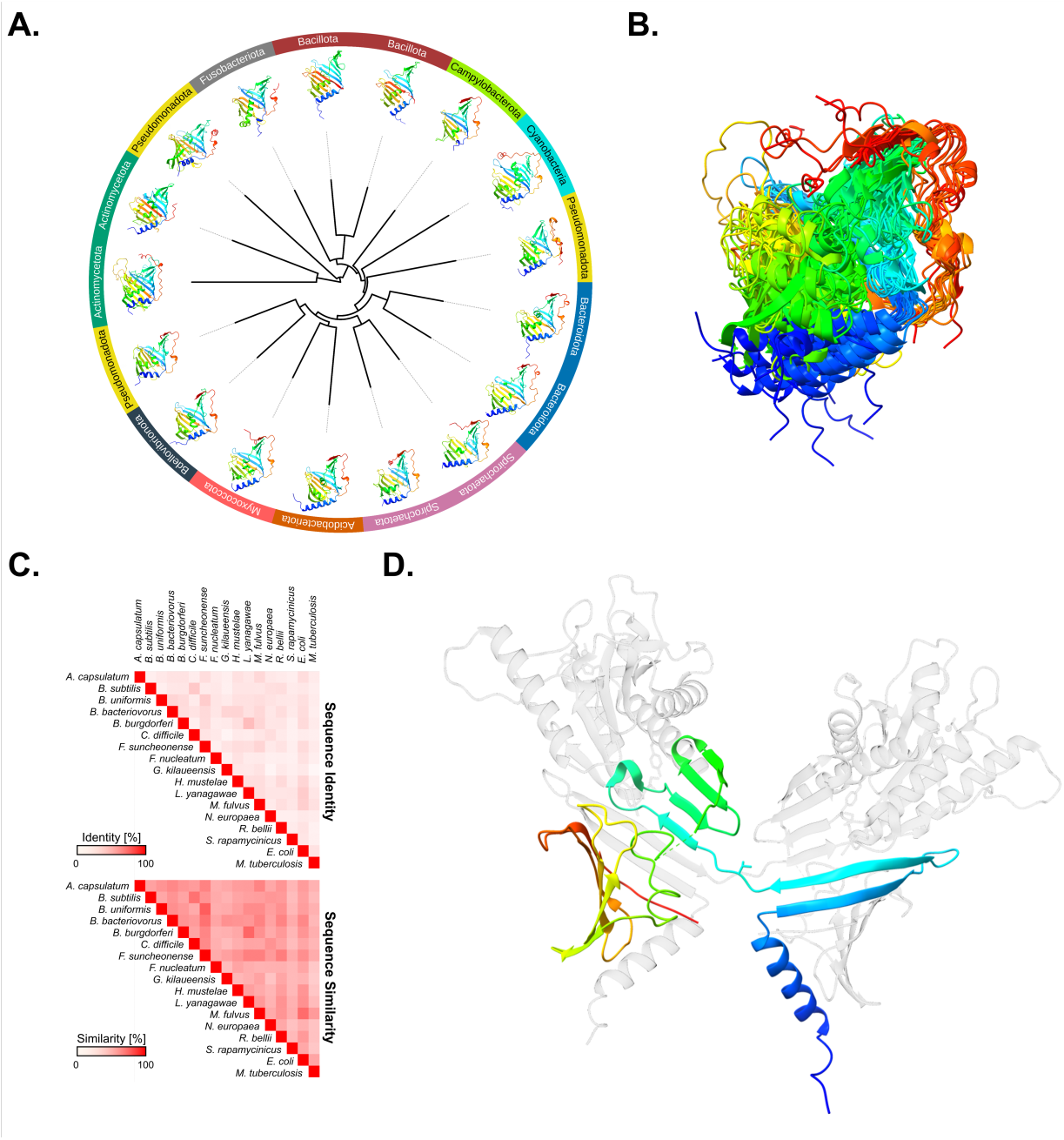

Figure 1. PLLLF proteins are structurally similar but share low sequence identity. A) Dendrogram generated by a DALI [43] structural alignment showing structural similarities of a subset of 17 crystal structures of PLLLF proteins. Bacterial orders to which each structure belongs are also shown. B) Structural alignment of the same subset of 17 crystal structures colored by residue. C) Comparisons of sequence identity and sequence similarity between 17 representative PLLLF proteins. Gradients represent percentages from 0 to 100. D) Crystal structure of the GerS-CwlD complex (7RAG) with GerS colored by residue to match the coloring of structures in panel B.

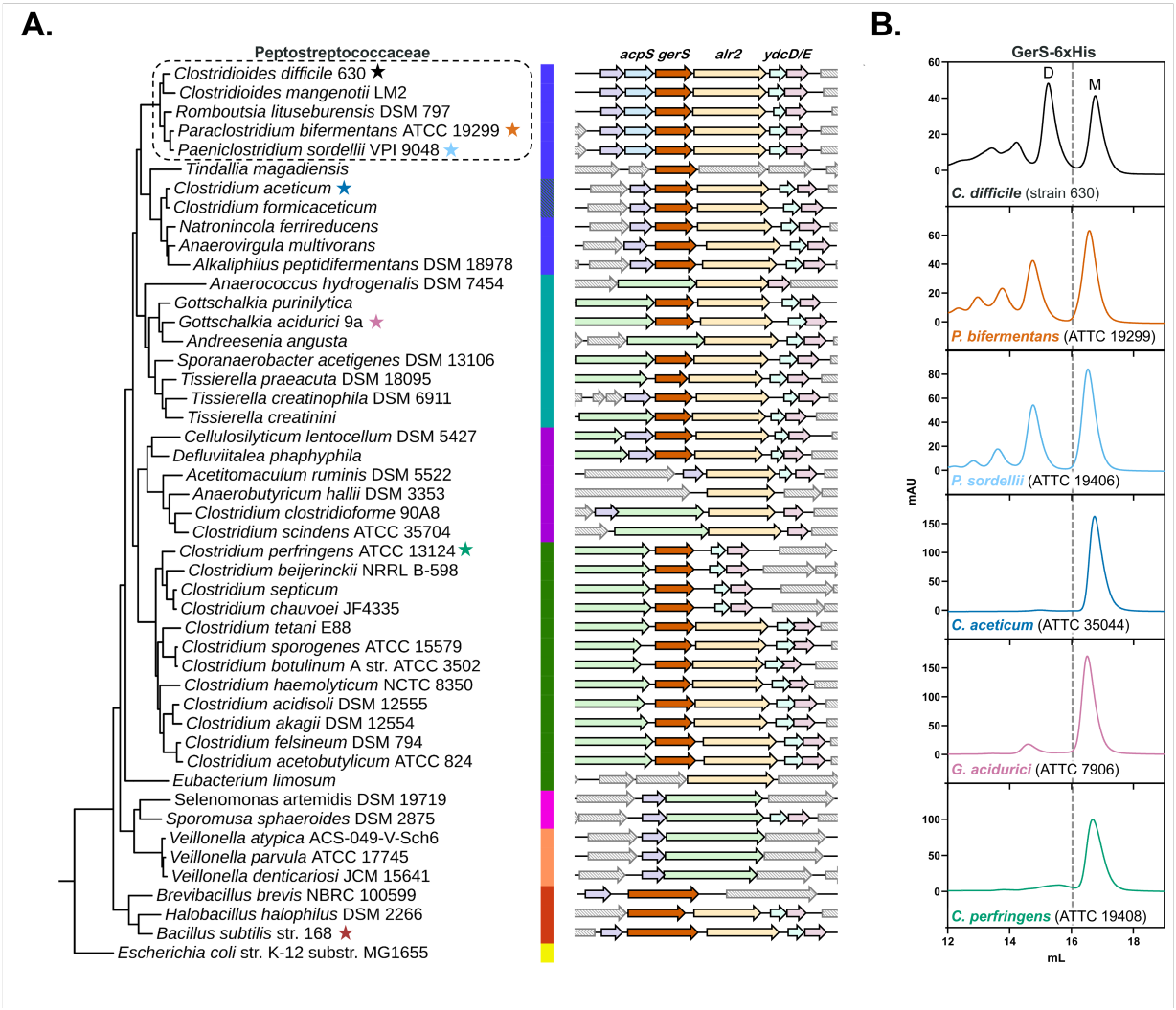

Figure 2. GerS dimerization is conserved to the Peptostreptococcaceae despite conservation of the protein throughout the Bacilliota phylum. A) Synteny analysis of the conserved GerS locus across orders in the Bacilliota phylum. Peptostreptococcales (blue), Tissierelliales (turquoise), Lachnospirales (purple), Eubacterales (green), Selenomonadales (pink), Vellionellales (orange), Bacillales (red), and the outgroup Enterbacterales (yellow). Colored stars correspond to representative GerS orthologs selected for SEC analysis. B) SEC analysis of GerS orthologs tagged with 6xHis for purification. Peaks are labeled with “D” for dimer or “M” for monomer.

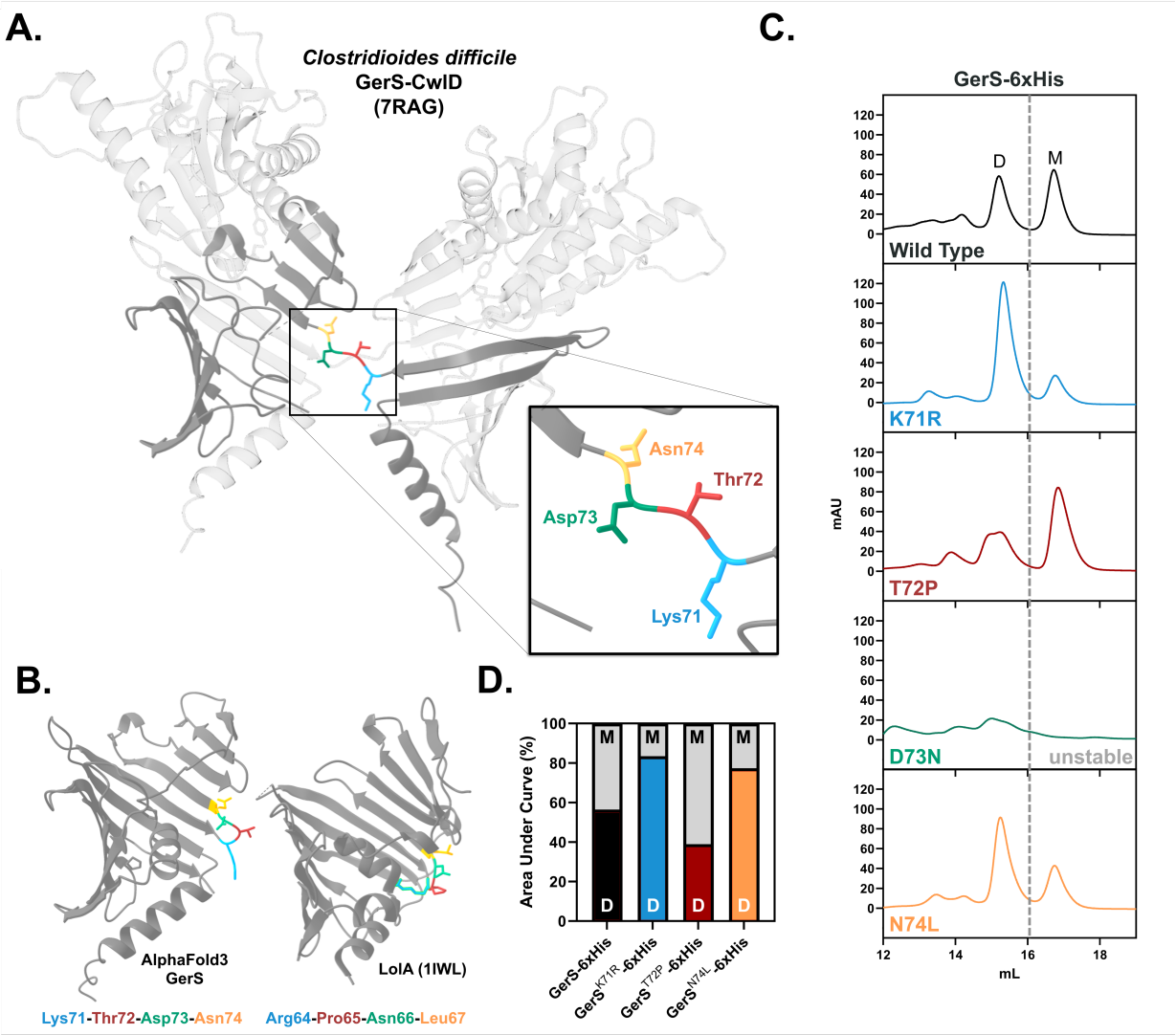

Figure 3. GerS hinge mutations guided by the LolA structure both stabilize and disrupt the GerS homodimer. A) Crystal structure of the GerS-CwlD complex. Hinge is colored by each residue. B) Aligned AlphaFold3 GerS structure and LolA (PDB - 1IWL). Hinge of GerS and analogous residues on LolA are colored by aligned residues. C) SEC traces of each GerS variant tagged with 6xHis. Peaks are labeled with either “D” for dimer or “M” for monomer. D) Ratios of areas under each peak. Column labeled “D” is the area under the dimer peak and column labeled “M” is area under the monomer peak. Ratios are represented as a percentage of total area of the monomer and dimer peaks combined.

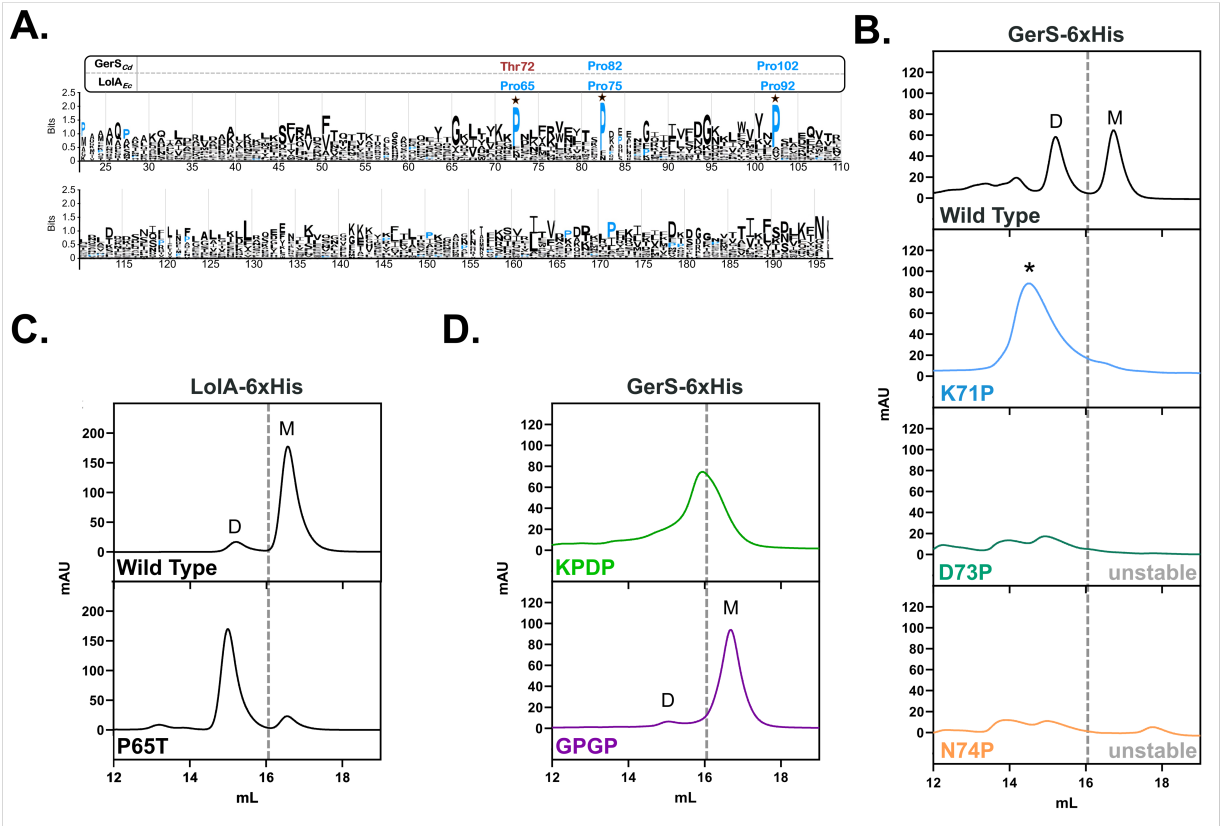

692

693 **Figure 4. Mutation of conserved proline in LolA promotes dimerization and introductions**
694 **of prolines into the hinge region of GerS disrupts dimerization.** A) Sequence logo depicting
695 amino acid propensity generated from DALI structural alignments of 17 representative PLLLF
696 proteins [43]. Prolines are highlighted in blue. Amino acids aligned to each conserved proline in
697 GerS and LolA are displayed. B) SEC traces of 6xHis-tagged GerS proline variants in non-
698 conserved locations (B), LolA and LolA^{P65T} (C), and dual proline GerS variants (D). Peaks are
699 labeled with either "D" for dimer or "M" for monomer.
700

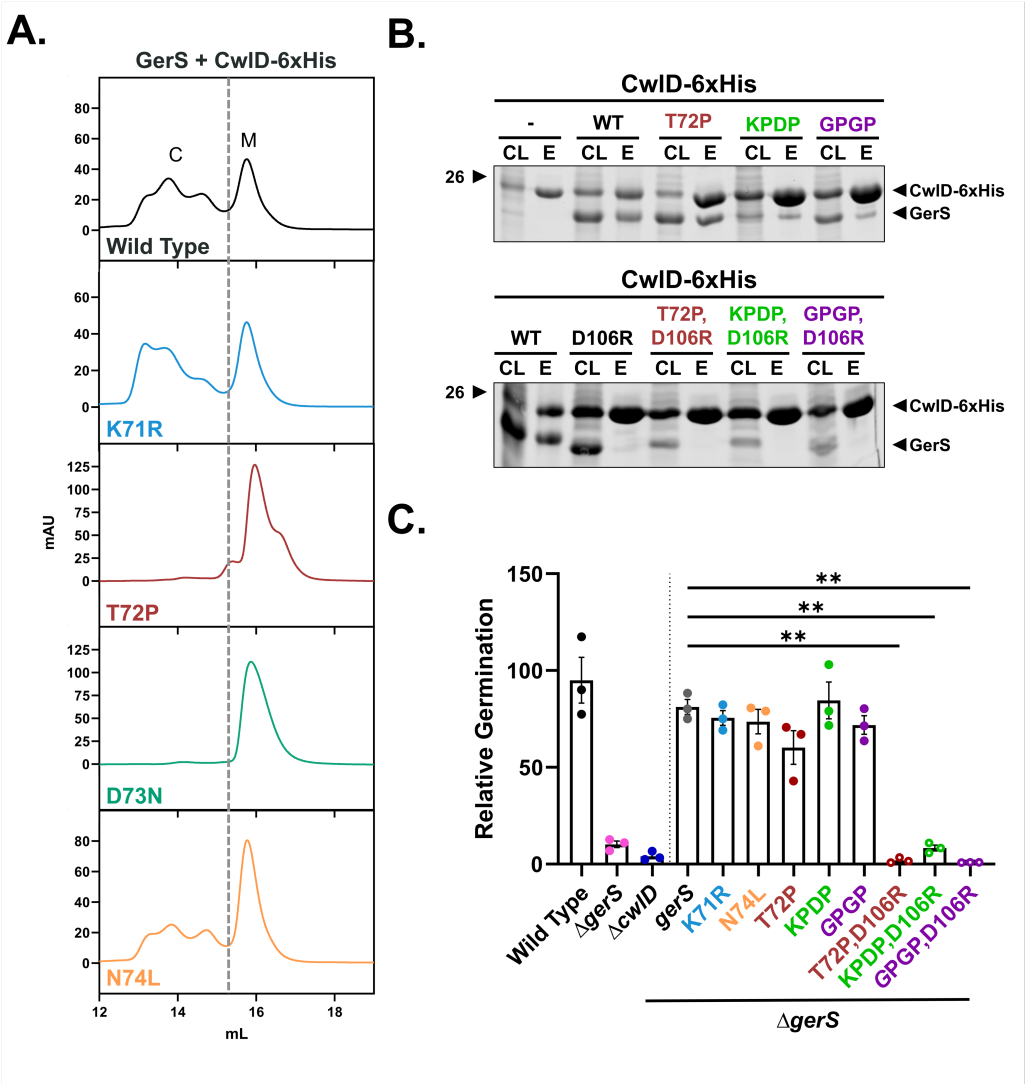

Figure 5. GerS variants disrupt interaction with CwlD and abolish spore germination. A) SEC traces of each LolA-guided GerS variant copurified with 6xHis-tagged CwlD. Peaks are labeled "M" for monomers or "C" for GerS-CwlD complex. B) Coomassie-stained cleared lysates (CL) and eluates (E) of untagged homodimer-disrupting GerS variants copurified with 6xHis-tagged CwlD. C) Relative germination calculated by area under the percent change in OD600 curve of spores in BHIS in the presence of 1% taurocholate over 1.5 hours. Each *gerS* mutant is expressed by its native promoter in the *pyrE* locus in a Δ*gerS* background. A one-way ANOVA followed by Dunnett's multiple comparisons test was used to compare each *gerS* mutant mean to the mean Δ*gerS*/*gerS* complement strain. Each mean is calculated from three biological replicates. Only significant differences are shown. (** $p < 0.005$).